REVIEW

PHOTOVOLTAICS

Photovoltaic materials: Present efficiencies and future challenges

Albert Polman,[1]* Mark Knight,[1] Erik C. Garnett,[1] Bruno Ehrler,[1] Wim C. Sinke[1,2]

Recent developments in photovoltaic materials have led to continual improvements in their efficiency. We review the electrical characteristics of 16 widely studied geometries of photovoltaic materials with efficiencies of 10 to 29%. Comparison of these characteristics to the fundamental limits based on the Shockley-Queisser detailed-balance model provides a basis for identifying the key limiting factors, related to efficient light management and charge carrier collection, for these materials. Prospects for practical application and large-area fabrication are discussed for each material.

Photovoltaics (PV), which directly convert solar energy into electricity, offer a practical and sustainable solution to the challenge of meeting the increasing global energy demand. In recent years, the decreasing price of PV systems has levelized the cost of PV-produced electricity to the point that it can now compete with the variable portion of consumer electricity prices in many countries worldwide: The point of "socket parity" has been reached (*1*). Substantial further cost reduction is needed, however, to allow PV to compete in more electricity markets and to enter the multi-terawatt regime. Aside from the solar cell and module fabrication costs, a major and increasing fraction of the cost of PV generation (typically 50%) is related to component and installation requirements such as inverters, cabling, mounting structures, and labor (*1*). As a result, solar cell efficiency is a key lever for PV cost reduction: For a given output power, a higher cell efficiency directly translates into a smaller and therefore less expensive PV system, reducing the levelized cost of electricity. A higher power generation rate per unit area is also important in urban environments where space is limited. The development of PV materials is experiencing an enormous growth, and efficiency records are continually broken. Below, we systematically compare the state of the art of the 16 most studied geometries of PV materials, with emphasis on the limitations of each material and its potential for further improvement and large-scale application.

Solar cells are made of semiconductor materials; given the broad solar spectrum, their fundamental efficiency limit is determined by several factors (Fig. 1). Photons with energies below the band gap are not absorbed, whereas photons with energies above the band gap are not fully converted to electrical energy because of thermalization of charge carriers (Fig. 1A, inset). Taking these two factors into account, ~45% of the incident spectrum-integrated solar power remains for semiconductors with a band gap of 1.1 to 1.4 eV. This is the maximum power that would be generated if the cell were operated at a voltage corresponding to the band gap energy and a current corresponding to full capture of all photons with energy above the band gap, followed by full collection of all generated carriers.

Even in an ideal case, however, the open-circuit voltage V_{oc} is always lower than the band gap energy because thermodynamic detailed balance requires the cell to be in equilibrium with its environment, which implies that there is spontaneous light emission from the cell. The corresponding radiative carrier recombination represents a dark current that causes V_{oc} to be well below the band gap voltage V_g (Fig. 1A, inset). Furthermore, under maximum-power operation (at maximum $J \times V$), the voltage V_{mp} is lower than V_{oc} and the current density J_{mp} is lower than the maximum (short-circuit) current density J_{sc} (Fig. 2A, inset). The efficiency limit that takes all these factors into account was first derived by Shockley and Queisser (S-Q) in 1961 (*2*). Figure 1B shows this limiting efficiency for a single-junction solar cell under "one-sun" illumination with the standard AM1.5 solar spectrum as a function of band gap; the maximum efficiency occurs for a semiconductor with a band gap of 1.34 eV and is 33.7%.

In practical solar cells, not all incident light is absorbed in the active layer(s) and not all generated carriers are collected; hence, J_{sc} is below the maximum value that can be achieved for a given band gap, E_g. The achievable V_{oc} is also reduced below the S-Q value by such phenomena as Auger recombination, band tail recombination, and recombination at bulk, interface, and surface defects (*3*–*5*). Furthermore, resistance and contact losses and other nonidealities reduce the fill factor $FF = (J_{mp}V_{mp})/(V_{oc}J_{sc})$. Combined, these factors lead to practical efficiencies that are often substantially lower than the S-Q limit for a given band gap.

Ideal and record-efficiency solar cells compared

We distinguish three classes of PV materials: (i) ultrahigh-efficiency monocrystalline materials with efficiencies of >75% of the S-Q limit for the corresponding band gap: Si (homojunction and heterojunction), GaAs, and GaInP; (ii) high-efficiency multi- and polycrystalline materials (50 to 75% of the S-Q limit): Si, $Cu(In,Ga)(Se,S)_2$ ("CIGS"), CdTe, methyl ammonium lead halide perovskite $[CH_3NH_3Pd(I,Cl,Br)_3]$, and InP; and (iii) low-efficiency materials (<50% of the S-Q limit): micro- or nanocrystalline and amorphous Si, $Cu(Zn,Sn)(Se,S)_2$ ("CZTS"), dye-sensitized TiO_2, organic and polymer materials, and quantum dot materials.

The record efficiency for each of these materials is plotted in Fig. 1B (see also table S1). The experimental values for J_{sc}, V_{oc}, and *FF* for the record-efficiency cell reported for each individual material are shown in Fig. 2, A to C, together with the limiting values calculated using the S-Q model (*2*). The experimental values for J_{sc} generally follow the trend given by the S-Q limit, with some materials closely approaching this limit. Values for V_{oc} and *FF* are much more scattered, with only a few materials approaching the S-Q limit. To analyze these trends, we evaluated two characteristic parameters for each material: (i) the current ratio $j = J_{sc}/J_{SQ}$, which indicates the degree of light coupling, absorption, and trapping in the active layer(s) of the cell, and also depends on the carrier collection efficiency; and (ii) the voltage ratio $v = V_{oc}/V_{SQ}$, which is primarily related to the degree of recombination of carriers in the bulk, surfaces, and interfaces. Together, the voltage ratio v and fill factor ratio $f = FF/FF_{SQ}$ indicate the total electrical limitations of a cell (*6*). A plot of j versus $v \times f$ for all evaluated materials (Fig. 3) directly indicates to what degree the cell efficiency is limited by light management or charge carrier management. Next, we describe these data for all materials.

Silicon (efficiency 25.0 to 25.6%)

Silicon has a nearly ideal band gap (E_g = 1.12 eV) for reaching high efficiency (Fig. 1). Si homojunction cells are based on a p-n junction made into either p-type or n-type Si(100) substrates. Several advanced device architectures and contacting schemes have been developed for Si solar cells. Contact recombination represents a major source of loss, so the most successful approaches minimize contact area (e.g., by localized heavy doping or metal deposition), implement passivated contacts, or use a combination of these approaches. In parallel, surface passivation of Si using Si_3N_4, Al_2O_3, SiO_2, or combinations of these materials has been developed to great perfection. The record efficiency for a monocrystalline Si homojunction cell was recently set at 25.1% (*7*) for a cell with a full-area tunnel oxide passivated rear contact and high-quality top surface passivation (the TOPCon design; Fig. 4A), slightly higher than the value of 25.0% (*8*, *9*) reported in 1998 for a cell

[1]Center for Nanophotonics, FOM Institute AMOLF, Science Park 104, 1098 XG Amsterdam, Netherlands. [2]Energy Research Center of the Netherlands (ECN), P.O. Box 1, Petten, Netherlands.
*Corresponding author. E-mail: a.polman@amolf.nl

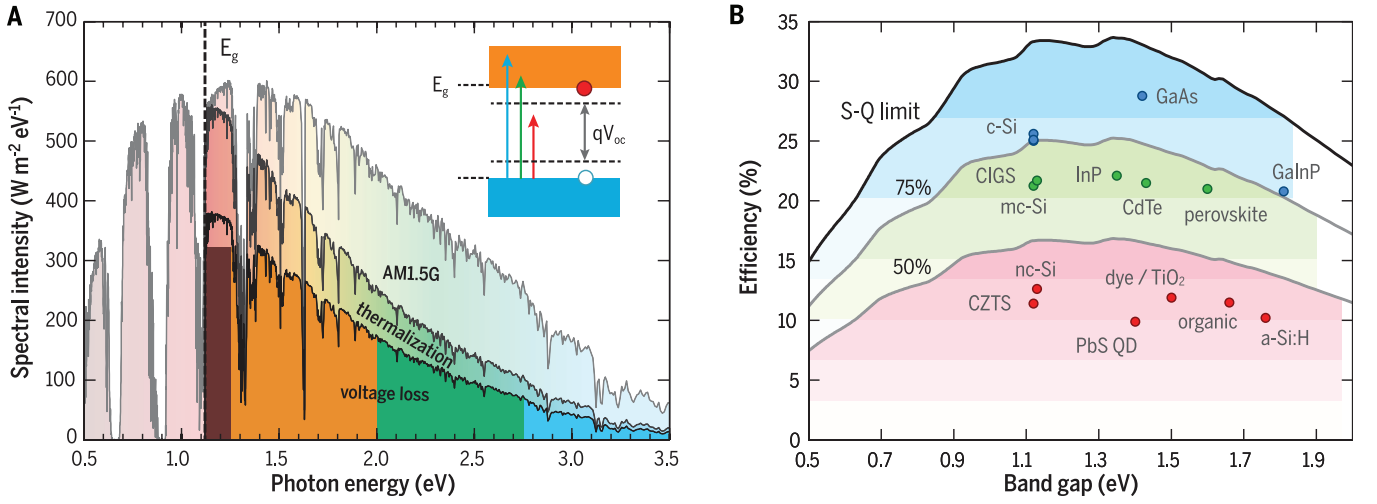

Fig. 1. Fundamental solar cell efficiency limits and present-day records. (**A**) AM1.5 solar spectrum with distinct dips due to molecular absorption in Earth's atmosphere. Photons with energies below the band gap (E_g, dashed black line corresponds to the band gap of Si) are not absorbed, whereas photons with energies above the band gap are not fully converted to electrical energy because of thermalization of charge carriers. The maximum power generated by the cell is limited by voltage loss relative to the band gap voltage. Inset: Electronic band structure with the separation of the quasi-Fermi levels determining the open-circuit voltage V_{oc}. (**B**) Theoretical Shockley-Queisser detailed-balance efficiency limit as a function of band gap (black line) and 75% and 50% of the limit (gray lines). The record efficiencies for different materials are plotted for the corresponding band gaps.

that used local contacts and high-quality surface passivation [the passivated emitter rear localized diffused (PERL) design].

The TOPCon cell has excellent current generation and collection (j = 0.96), similar to the value achieved for two other record-efficiency Si solar cell designs (table S1). This results from a combination of very low surface reflection [achieved by a pyramidal (111)-faceted surface texture combined with an anti-reflection coating (ARC)] and very low recombination losses in the Si wafer and at the surfaces and contact interfaces. Low recombination is also reflected in the relatively high voltage of the TOPCon cell (v = 0.82).

In a radically different design, both the p-n junction and the contacts are placed at the rear of the cell. This interdigitated back-contact (IBC) design features alternating p-type and n-type contact regions (Fig. 4B). The IBC design eliminates front contact shading losses and reduces series resistance by allowing more metal to be used for current collection and transport. This comes at the cost of more challenging carrier transport in the device (carriers generated near the surface must be collected at the back) and requires the use of very high-quality material. Overall current generation and collection in the IBC cell is slightly lower than in the TOPCon cell (j = 0.95 versus 0.96), as is the record efficiency (25.0% versus 25.1%) (*9*–*11*). Note that the IBC cell has an area of 120 cm^2, whereas the TOPCon cell measures 4 cm^2. The IBC cell uses a doped surface layer, which creates a front surface field that repels carriers from the surface, and has a Si_3N_4 top layer that serves as both an ARC and a high-quality passivation layer for the Si surface. The lower surface and bulk recombination rates lead to a slightly higher voltage (v = 0.83) for the IBC cell relative to the TOPCon cell.

An efficiency record of 25.6% was recently reported for an IBC Si solar cell that uses silicon heterojunctions (SHJs) rather than homojunctions for carrier collection (*9*, *12*). In this approach, a thin stack of doped and intrinsic hydrogenated amorphous Si (a-Si:H) layers is deposited onto a crystalline Si surface to form a junction, replacing the process of junction formation by high-temperature dopant diffusion (Fig. 4C). The SHJ design avoids carrier recombination in highly doped p-type and n-type regions and is made using a low-temperature process, which better preserves the minority carrier lifetime of the Si wafer. The surface of the record SHJ cell is passivated with a-Si:H. This design led to the highest voltage observed for a Si solar cell (v = 0.84). The overall result of carrier generation and collection is similar to that of the TOPCon cell (j = 0.96). The origins of the small remaining losses in these high-efficiency Si cells are quite different because of their different design and mode of operation.

As a result of the indirect band gap of Si, the absorption coefficient is relatively low and varies only gradually around the band gap energy, so that a relatively thick wafer is required to absorb all light with photon energies above the band gap. This, however, leads to higher bulk (Auger) recombination and thus reduces V_{oc}. Moreover, it increases the material costs. The present tradeoff among cost, manufacturability, and performance leads to an optimum Si wafer thickness of 100 to 200 μm for commercial cells. These wafers are made by diamond wire sawing from monocrystalline Si rods produced by Czochralski crystal growth.

Multicrystalline Si wafers are cut from cast ingots produced using directional (unseeded or seeded) crystallization, and their fabrication cost is lower than that of monocrystalline wafers. The typical grain size depends on the growth method and can be as large as several centimeters. Multicrystalline Si has a lower electronic quality, due to crystal grain boundaries and intragrain defects, as well as a higher concentration of impurities. As a result, the record-efficiency multicrystalline Si cell has large voltage loss (v = 0.76). Light trapping in these cells is less efficient because the ideal pyramidal surface texture normally formed by alkaline-etching Si(100) to the (111) surface facets cannot be realized on a multicrystalline surface. This, together with incomplete carrier collection due to recombination, leads to a reduced current (j = 0.91). Together, these voltage and current losses yield a lower efficiency (20.8%) (*9*, *13*) than for monocrystalline Si cells. The record-efficiency multicrystalline Si cell has a passivated emitter and rear cell (PERC) p-n junction design (Fig. 4D).

According to the S-Q model, the efficiency limit for Si solar cells is 33.3%, far above the experimental record of 25.6%. A key limiting factor that is not accounted for in the S-Q model is Auger recombination of free carriers that occurs under illumination. Taking this into account for Si, the efficiency limit for an undoped (monocrystalline) Si cell with optimized thickness (110 μm) was calculated to be 29.4% (*14*), leaving room for further development of existing technologies in the coming years.

Today the global PV market is dominated by wafer-based crystalline Si solar modules, with a total market share of >90%. Multicrystalline Si represents ~65% and monocrystalline Si ~35% of this market segment (*15*). PV systems based on Si solar cells installed in the field have been shown to offer high reliability and very limited efficiency degradation over a period longer than 25 years.

GaAs (efficiency 28.8%)

The record efficiency for a single-junction solar cell under one-sun illumination has been achieved using GaAs (28.8%) (*9*, *16*). This material has a direct band gap close to the optimum (1.42 eV; Fig. 1). Because of the high optical absorption coefficient of GaAs, the cell thickness can be kept relatively small (~2 μm) to harvest the solar spectrum

up to the band gap. The record-efficiency cell design has a n-GaAs/p-$Al_{0.3}Ga_{0.7}As$ junction geometry with high–band gap window layers that serve to retain minority carriers in the GaAs active layer (Fig. 4E). The GaAs heterostructure is epitaxially grown using chemical vapor deposition, which is a relatively energy-intensive process. Interestingly, the record efficiency was achieved using a lift-off process, in which a GaAs foil ~2 μm thick was exfoliated from the substrate (by chemical etching of an AlAs buffer layer) and laminated onto a Cu substrate. The voltage of the record-efficiency cell is very high (v = 0.97). Light reflection, top-finger shadowing, incomplete light trapping, and absorption in the metal back contact result in some current loss (j = 0.92), leaving room for improvement. Application of an IBC geometry, for example, could potentially further increase j. An intermediate dielectric back-reflecting geometry can reduce parasitic absorption in the metal back contact. The fill factor in these cells is very high (f = 0.97). Taking into account Auger recombination, the maximum efficiency that can be achieved for a practical single-junction GaAs cell is ~32% (*17*), substantially greater than the current record value.

Whereas III-V solar cells have traditionally been used in niche markets requiring high efficiency on a small area, such as space technology, the newly developed layer-transfer technology enables fabrication of large-area flexible (single-junction) GaAs technology at reduced cost for a much broader range of applications. Encapsulation and recycling of commercial GaAs modules is important because of the use of the toxic element As.

InP (efficiency 22.1%) and GaInP (efficiency 20.8%)

Two other III-V compound semiconductors that have achieved high efficiencies are InP and GaInP. InP (E_g = 1.35 eV) has a band gap similar to that of GaAs, but the maximum reported efficiency of 22.1% (*9*, *18*) is much lower than for GaAs; this difference is due to both lower voltage and lower current (v = 0.81, j = 0.85). Because of the existing high-efficiency GaAs alternative and the scarcity and associated high cost of In, developments on InP cells have been minimal in the past decade. GaInP has a relatively high band gap (1.81 eV), for which the S-Q limit efficiency is 25.2%. The record efficiency achieved for a GaInP cell is 20.8% (*9*, *19*). The voltage loss on the record cell is extremely small (v = 0.96), but current collection (j = 0.82) in these cells leaves much room for improvement. The record-efficiency GaInP cell has the highest fill factor achieved for any material (FF = 0.89; f = 0.98), which is partly related to the high band gap (Fig. 2C). Because of its large band gap, GaInP is used in III-V multijunction solar cell geometries. Recently, a mechanically stacked tandem composed of a GaInP top cell and a Si heterojunction base cell was reported with an efficiency of 29.8% (*11*).

CIGS (efficiency 21.7%)

The record efficiency of $Cu(In,Ga)(Se,S)_2$ (CIGS) thin-film solar cells has steadily increased over the past 20 years, with the present record value at 21.7% (*9*, *20*), making it the highest-efficiency thin-film solar cell material to date, very closely followed by CdTe at 21.5% (*9*, *21*). CIGS has a chalcopyrite crystal structure and its band gap can be continuously tuned between ~1.0 and 2.4 eV by varying the In/Ga and Se/S ratios, with the low–band gap compositions so far always giving the best performance. Polycrystalline films of CIGS are made using sputtering or evaporation from the constituent elements and are typically deposited onto a Mo film that is sputtered on a soda-lime glass substrate. The typical active layer thickness is ~2 to 3 μm. Sodium diffusing from the glass substrate into the CIGS layer has been found to play a key role in passivating defects in the CIGS layer; the record cell also incorporated traces of K. The CIGS composition is typically graded to form an electric field that repels minority carriers from the Mo back contact, which is a strong recombination sink. The cell is finalized by the chemical-bath deposition of CdS to form a heterojunction followed by an intrinsic ZnO buffer layer, a transparent ZnO:Al conducting layer (TCL), and a MgF_2 ARC (Fig. 4F). In some recent high-efficiency devices, the CdS layer is replaced by the more transparent ZnO_xS_{1-x}. Indium is a key element in CIGS, and its scarcity is a concern for scaling up CIGS module production to the terawatt level.

The voltage for the record-efficiency CIGS cells (E_g = 1.13 eV) is very high, with v = 0.84, equal to the best monocrystalline Si cells. Given the polycrystalline nature of the material, this implies that grain boundaries in this material do not act as strong carrier recombination sites. There is substantial current loss (j = 0.84) due to light reflection, incomplete light trapping, absorption in the Mo back contact, and parasitic absorption in the CdS and ZnO:Al layers. The absorption spectrum of CIGS shows a rather gradual variation with energy around the band gap, which leads to unavoidable current loss in the near–band gap spectral range. As with all polycrystalline materials, improving material quality is a complex process that requires optimization of many different parameters such as deposition conditions, (post-)annealing procedures, and ambients. Because of the complex stoichiometry of CIGS, many secondary phases are possible, and much of the progress in efficiency has been achieved by optimizing the deposition and annealing process to avoid such detrimental by-products. Creating a good ohmic electrical contact between Mo and CIGS (via a $MoSe_2$ interfacial layer) is another important factor. Replacing the CdS buffer layer with a nontoxic and more transparent material is also a key research area.

The possibility of band gap tuning makes CIGS an interesting material in tandem solar cells, either by combining CIGS layers with different band gaps or by using a high–band gap CIGS top cell on top of a Si base cell. So far, however, high–band gap (Ga-rich) CIGS cells have not yielded sufficient efficiencies for a CIGS/Si tandem to beat the record-efficiency Si cell.

CdTe (efficiency 21.5%)

CdTe is a binary semiconductor with a cubic zincblende crystal structure and a near-ideal band gap of 1.43 eV. It can be deposited at relatively low temperature using evaporation from CdTe powder. Cells are typically grown in a superstrate configuration starting from a glass substrate coated with fluorine-doped tin oxide (FTO). The subsequent layer stack usually consists of CdS (generally deposited by chemical bath deposition), followed by evaporated CdTe (thickness typically 2 to 3 μm)

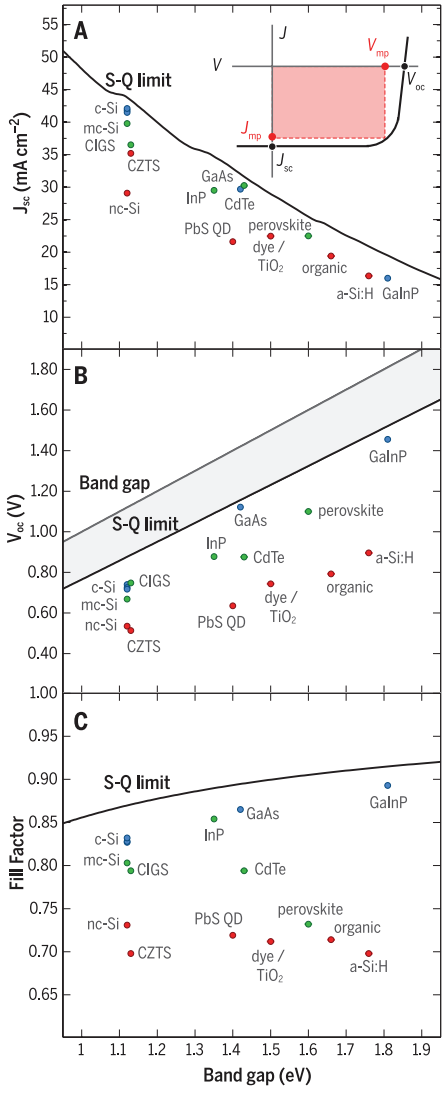

Fig. 2. Record-efficiency cell parameters compared to the detailed-balance limit. Single-junction solar cell parameters are shown as a function of band gap energy according to the Shockley-Queisser limit (solid lines) and experimental values for record-efficiency cells. (**A**) Short-circuit current J_{sc}. Inset: A typical current-voltage $J(V)$ curve, with V_{oc}, J_{sc}, V_{mp}, and J_{mp} indicated. The product of current and voltage is highest at the maximum power point ($J_{mp}V_{mp}$). (**B**) Open-circuit voltage V_{oc}. The voltage corresponding to the band gap is shown for reference, with the voltage gap V_g-V_{SQ} indicated by the gray shaded region. (**C**) Fill factor $FF = (J_{mp}V_{mp})/(V_{oc}J_{sc})$. All data are for standard AM1.5 illumination at 1000 W/m^2.

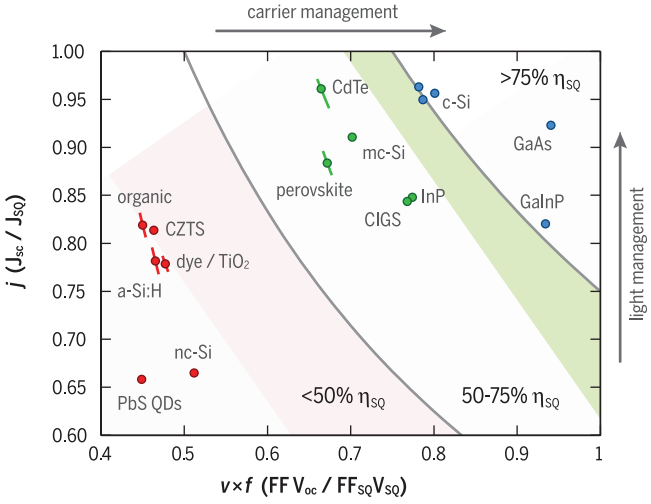

Fig. 3. Fraction of Shockley-Queisser detailed-balance limit for voltage and current achieved by record cells. The current ratio $j = J_{sc}/J_{SQ}$ is plotted versus the product of the voltage and fill factor fractions ($v \times f = FF\ V_{oc}/FF_{SQ}V_{SQ}$) for the record-efficiency cells of all evaluated materials. The lines around some data points correspond to a range of band gaps taken in the S-Q calculations according to uncertainty in the band gap of the record cell. Arrows on top and right axes indicate how improved light management and charge carrier collection improve the cell efficiency. η_{SQ} denotes maximum achievable efficiency according to the SQ model.

and a metal back contact such as Al or Ti, in some cases with a CuZnTe interfacial layer between the metal and the CdTe (Fig. 4G).

The highest reported certified efficiency for CdTe is 21.5% (*9*, *21*), although for the purpose of this review we analyze cells with the previous record of 21.0% (*22*) because detailed data for the new record-efficiency cell are not yet available. The steep absorption coefficient versus energy for CdTe enables very good current collection in CdTe cells ($j = 0.96$), far superior to any other thin-film technology and equal to that of the record-efficiency monocrystalline Si cells. The high voltage loss in CdTe cells ($v = 0.75$) is attributed to recombination losses in the crystal grains and at interfaces in the polycrystalline material; the exact nature of this recombination is still unclear.

CdTe solar modules are commercially produced by several companies and have the largest market share among present thin-film technologies, which are dominated by CdTe, CIGS, and thin-film Si. Recycling systems have been set up for commercial CdTe modules, which is particularly important because of the use of the toxic element Cd; the scarcity of Te is also a concern.

Methyl ammonium lead halide perovskite (efficiency 21.0%)

Hybrid organic-inorganic perovskite solar cells have recently taken the PV research world by storm, with efficiencies above 20% achieved after only 5 years of substantial work. These materials have the general formula ABX_3, where A is an organic cation (most often methylammonium, CH_3NH_3), B is an inorganic cation (usually Pb), and X is a halide [typically I, often with a small fraction of Cl or Br: $CH_3NH_3Pb(I,Cl,Br)_3$]. Depending on the halide used, the band gap can be continuously tuned from ~1.6 eV (pure I) to 3.2 eV (pure Cl), with the smaller–band gap materials providing better solar cell efficiencies (*23*). Even smaller band gaps can be achieved using a different organic cation (e.g., formamidinium, H_2NCHNH_2) or inorganic cation (e.g., Sn), and such compounds are desirable as they have a higher efficiency limit (Fig. 1B).

The perovskite salts form polycrystalline films with a perovskite structure at or near room temperature by precipitation from a variety of polar solvents (commonly dimethyl formamide or dimethyl sulfoxide). The device geometry is usually very similar to, and inspired by, those used for solid-state dye-sensitized or polymer bulk heterojunction solar cells. Typically, an FTO-coated glass substrate is coated with an electron-selective contact (usually TiO_2). Subsequently, the perovskite is deposited either by spin-coating the soluble precursors (methyl ammonium iodide and lead iodide, bromide, or chloride) or evaporating the constituent powders. A low-temperature annealing process (<150°C) often helps to improve crystallinity, film morphology, and device performance. Finally, the hole-selective top contact (usually Spiro-OMeTAD, $C_{81}H_{68}N_4O_8$) is spin-coated on top, and the back contact (usually gold) is evaporated to finish the device (Fig. 4H).

The record perovskite solar cell efficiency is 21.0% (*9*, *24*), although for the purpose of this review we analyze cells with the previous record of 20.1% (*9*, *24*) because detailed data for the new record cell are not yet available. This cell has a very small area and exhibits a relatively small voltage loss ($v = 0.83$), even better than the record-efficiency monocrystalline Si homojunction cells, which is remarkable for a solution-processed semiconductor. Even though the absorption spectrum of perovskites shows a very sharp onset, comparable to that of the best semiconductor absorbers (CdTe and GaAs), the photocurrent loss is still substantial ($j = 0.88$). This loss comes primarily from parasitic absorption in the hole-conducting layer and the back reflector. The fill factor in these cells ($FF = 0.73$; $f = 0.81$) is the lowest of all cells with efficiencies greater than 20%, most likely because of a combination of nonuniformity in the absorber (e.g., pinholes) and carrier-selective contacts that lead to carrier shunting, along with resistive losses associated with nonideal carrier-selective contacts. The fill factor (and thus the efficiency) is expected to continue to increase as these factors are optimized further.

Despite their excellent initial performance, hybrid perovskite solar cells are known to degrade within a few hours to days under standard operating conditions; at present this is the greatest barrier to commercial implementation. The origins of perovskite cell instability are currently a topic of active research, although photoreduction by ultraviolet light and reactions with water have already been identified as likely candidates. Also, measurements of the current-voltage characteristics can suffer from hysteresis, making efficiency analysis complex. The origin of this hysteresis is still unclear, but the leading hypothesis involves ion (or vacancy) migration under operating conditions. The perovskite salts are partially soluble in water, so the cells are sensitive to humidity. Because of Pb toxicity, encapsulation and recycling are important for this technology to become viable for large-scale application. The toxicity challenge is greater for this material than for CdTe and GaAs because the much higher water solubility and lower vaporization temperature make environmental exposure during module encapsulation failure (breakage, fire) more dangerous. Large–band gap perovskites may serve as a top cell in Si/perovskite tandem solar cells that have a potential efficiency above 30%; such an application provides a possible entry point to the market for the perovskite technology and is currently under intense research.

CZTS (efficiency 12.6%)

$Cu(Zn,Sn)(S,Se)_2$ (CZTS) is a solar cell material similar to CIGS, but with the scarce element In replaced by Zn and Ga replaced by Sn. CZTS can crystallize to form either a kesterite or stannite crystal structure, with kesterite being preferable for PV applications. As in CIGS, the band gap of CZTS can be tuned over a substantial range (1.0 to 1.6 eV); the best results have been achieved for a Cu-poor, Zn-rich stoichiometry with the band gap controlled by the S/Se ratio (*25*). The cell structure is nearly identical to what is used for CIGS. Cell fabrication can also follow a similar process, although the record-efficiency CZTS cells have been made using solution deposition of chalcogenides dissolved in hydrazine followed by annealing in selenium vapor. The record CZTS cell has an efficiency of 12.6% (*9*, *26*) and suffers from large voltage loss ($v = 0.58$) due to recombination at defects in the bulk material and at the charge extraction interfaces. As with CIGS, the complex nature of the material requires study of many different types of defects and careful engineering of the fabrication and device processing to minimize the most detrimental defects. Controlling interfacial reactions at the Mo metal contact is crucial for reducing interfacial recombination and minimizing series resistance. Current loss in CZTS cells is comparable to that of CIGS ($j = 0.81$). Finding an alternative back contact with lower optical loss (higher reflectivity) that can withstand the full device processing and maintain low series resistance would be a major breakthrough in the development

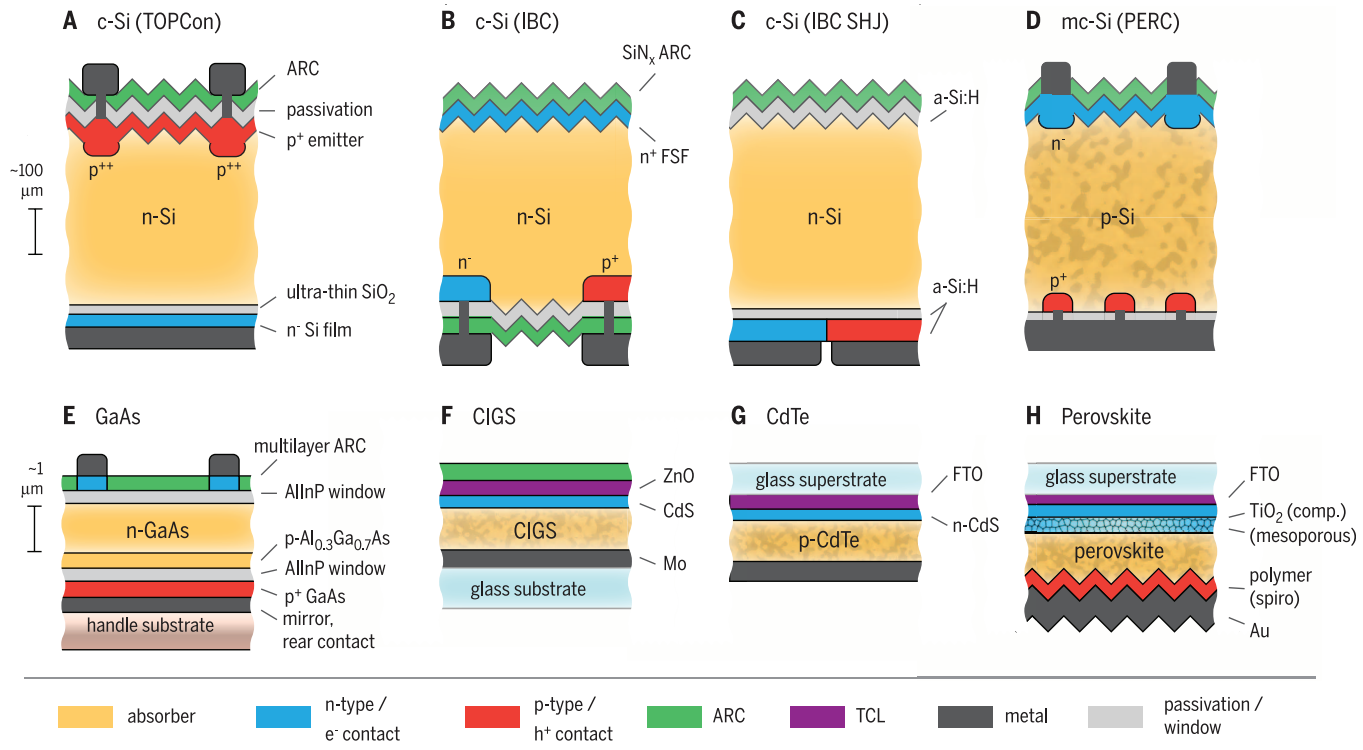

Fig. 4. Layer and contact geometry for solar cells with record efficiencies above 20%. (**A**) TOPCon crystalline Si (Fraunhofer). (**B**) IBC crystalline Si (SunPower). (**C**) Heterojunction IBC crystalline Si (Panasonic). (**D**) Multicrystalline Si (Trina Solar). (**E**) GaAs thin film (Alta Devices). (**F**) CIGS thin film (ZSW Stuttgart). (**G**) CdTe thin film (First Solar). (**H**) Perovskite thin film (KRICT). For industrial cells, the exact geometry is not publicly available.

of CZTS solar cells, although the biggest factor limiting efficiency is the low V_{oc}, a consequence of the relatively poor material quality.

Dye-sensitized solar cells (efficiency 11.9%)

Dye-sensitized solar cells are a special class of devices, as they involve an electrochemical power generation process. In these cells, the absorber is not an extended solid semiconductor but a molecular dye (typically a ruthenium organometallic complex, although zinc porphyrin and even purely organic dyes have also given very high efficiencies) that is coated onto a highly porous nanostructured electrode (typically TiO_2). The photoexcited dye injects electrons into the conduction band of the TiO_2 and accepts electrons from a redox couple (typically I^-/I^{3-}, although higher voltages have been reached with Co-based redox couples) in a nonaqueous electrolyte. The redox active species must then diffuse to the counter electrode (usually Pt or graphite) to be regenerated and complete the current circuit. Dye-sensitized solar cells are made by depositing a very thin compact TiO_2 layer typically on FTO, followed by formation of mesoporous TiO_2 by printing a TiO_2 nanoparticle paste, annealing, $TiCl_4$ treatment to passivate surface traps, and finally dye adsorption by immersion in solution. A glass plate covered with the counter electrode is brought very close to the substrate using spacers, and the cell is filled with electrolyte and sealed. Here, we analyze these cells according to the S-Q model, which assumes a semiconductor absorber with an absorption band edge; although this is not the case for dye-sensitized cells, the numbers for v and j then provide a reference relative to a conventional semiconductor with a band gap equal to the peak of the dye absorption spectrum (1.50 eV).

The record dye-sensitized cell has an efficiency of 11.9% (*9*, *27*) with a large voltage loss (v = 0.60) due to the relatively low potential of the standard I^-/I^{3-} redox couple, which introduces a large energy loss when transferring electrons to the dye. No better dye-based alternatives have been found despite intense research over the past several years: Redox couples with higher potentials either react too quickly with electrons injected into the TiO_2 (leading to recombination) or are too bulky for rapid ionic diffusion through the electrolyte (leading to strong losses in the fill factor at high light levels).

An additional challenge for dye-sensitized solar cells is the relatively high energy and narrow bandwidth associated with molecular absorption, which makes it difficult to harvest a wide range of the solar spectrum (j = 0.78). Using multiple dyes introduces complications with the redox chemistry, whereas using dyes with broader spectra reduces oscillator strength and requires porous electrodes to become too thick for efficient charge extraction. Despite these difficulties, dye-sensitized solar cells have already been commercialized because of their relatively simple fabrication, low-cost materials, and availability in a variety of colors and opacities that are useful when aesthetics are important. Moreover, dye-sensitized solar cells have served as a model system or inspiration for the development of a new class of nanostructured device architectures for PV solar energy conversion and solar fuel generation.

Organic solar cells (efficiency 11.5%)

Organic solar cells offer inexpensive roll-to-roll fabrication on flexible substrates and a wide choice of materials for applications where flexibility and color are important. Organic solar cells come in two varieties: sublimed small-molecule solar cells and solution-processed polymer/fullerene solar cells. The highest reported certified efficiency for a single-junction organic solar cell is 11.5% (*28*, *29*), although for the purpose of this review we analyze cells with the previous record of 11.0% (*9*, *30*) because detailed data for the new record-efficiency cell are not yet available. The previous record was achieved using a polymer with a 1.66-eV band gap.

Polymer solar cells are typically prepared on ITO-coated glass or foil with the active polymer donor–fullerene acceptor blend sandwiched between a hole-selective layer [typically poly(3,4-ethylenedioxythiophene) polystyrene sulfonate (PEDOT:PSS) or MoO_3] and an electron-selective layer such as ZnO, TiO_2, or a low–work function material such as Ca. The typical active layer thickness is ~100 nm.

Because of the low dielectric constant of organic materials, photogenerated electron-hole pairs remain tightly bound, necessitating the use of dedicated architectures such as bulk heterojunctions to achieve efficient charge separation and extraction. The energy offsets needed for the heterojunction to ensure efficient exciton dissociation lead to a voltage loss of ~0.3 eV in practice, which lowers the efficiency by about 2% absolute (*31*). Currently,

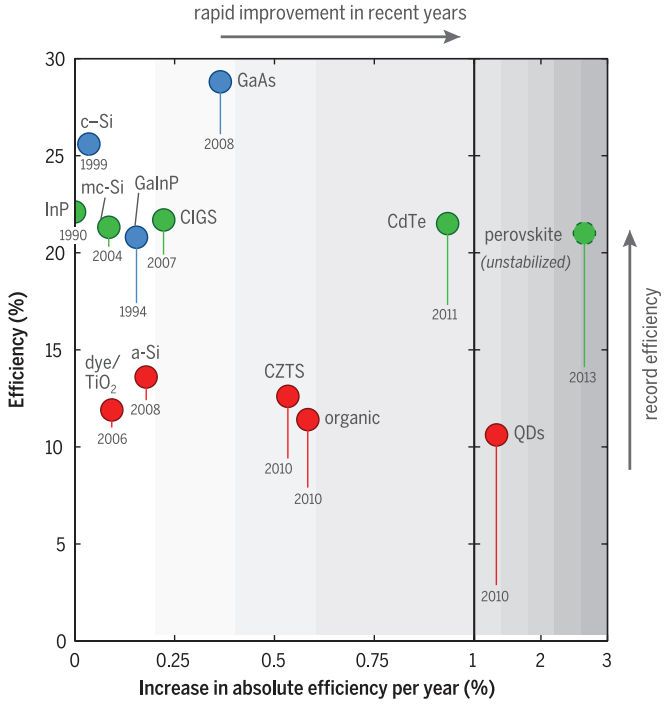

Fig. 5. Rates of improvement in solar cell efficiency over recent years. Average improvements were calculated over a period ending 1 January 2016 and starting with the date of the last record preceding 2010 [with two exceptions: perovskites (starting 2013, when the first certified efficiency was reported) and CdTe (starting 2011, as no recent record before 2010 was available and much progress occurred after 2010)]. Progress in efficiency from the pre-2010 record to the current values is indicated by the vertical lines. Colors correspond to cells achieving <50% of their S-Q efficiency limit (red), 50 to 75% (green), or >75% (blue). This analysis is based on data from the National Renewable Energy Laboratory efficiency chart, Green's tables, and publications (*11*, *19*, *29*).

the limiting problems for organic solar cells are the high rate of nonradiative recombination (via trap states or triplet excited states) and the large degree of static and dynamic disorder, together yielding very large voltage loss (v = 0.57). To a large extent, this voltage loss could be overcome by direct optical excitation of the charge-transfer state between electron donor and electron acceptor. So far, common material combinations show a very low oscillator strength of these charge-transfer states, rendering direct optical excitation nearly absent. Substantial current loss (j = 0.82) is due to parasitic absorption by the selective contacts, incomplete absorption by the polymer, and incomplete carrier collection resulting from nonradiative recombination (low mobility and diffusion length).

As with thin-film Si solar cells, organic PV technology is suffering from the fact that efficiency is becoming an increasingly important driver to reduce the cost of large-area PV systems. Also, organic cells often show degradation under illumination. At the same time, a variety of attributes—relative ease of processing, nontoxicity, low weight, potential for low cost, and possibility of forming flexible modules of many different shapes, colors, and transparencies—enables applications that may not be achievable with thin-film flexible CIGS, CdTe, or perovskite cells that have much higher efficiency.

Thin-film silicon (efficiency 10.1 to 11.4%)

Thin-film microcrystalline or nanocrystalline Si solar cells can be made on a wide range of (flexible) substrates by means of chemical vapor deposition. Typically, a p-i-n geometry is grown on a ZnO:Al-coated textured glass substrate, followed by a ZnO:Al buffer layer and Ag back contact. The record efficiency is 11.4% (*9*, *32*). The relatively slow deposition rate of crystalline Si limits the cell thicknesses that can be practically achieved to 2 to 5 μm, and the textured substrate often leads to defected growth of the microcrystalline film. As a result of this thickness limitation, light with energies near the band gap is not fully absorbed, leading to a very strong current penalty with j = 0.67, the lowest value of all cells reviewed here. Crystal grain boundaries and other defects in deposited micro- or nanocrystalline Si cells are strong sinks for minority carriers, leading to a large voltage loss as well (v = 0.61).

Amorphous Si (a-Si:H) is a semiconductor with much stronger optical absorption than crystalline Si, but with a band gap well above the optimum (1.7 to 1.8 eV). It is made using vacuum deposition techniques, typically at a much higher rate than micro- or nanocrystalline films. Despite the incorporation of hydrogen in these films to passivate bulk defects, the electronic quality of this material is rather low, with a correspondingly large voltage loss (v = 0.61) for the record-efficiency single-junction cell (10.2%) (*9*, *33*). In a-Si:H cells, the optimum efficiency is strongly determined by the trade-off between cell thickness and carrier collection efficiency: A large thickness is required to optimize the capture of incident light, but this reduces the carrier collection efficiency if the cell is thicker than the carrier drift/diffusion length, which is typically a few hundred nanometers; for the record-efficiency cell, j = 0.78. Amorphous Si cells are most often fabricated in a superstrate configuration using a textured glass substrate coated with ITO as a transparent conductor. This then forms the starting point for the subsequent growth of a-Si:H, ZnO:Al buffer layer, and Ag back contact.

As cell efficiency becomes an increasingly important factor in PV cost reduction, the progress of thin-film Si technology has slowed in recent years. Yet the possibility of fabricating flexible modules using a roll-to-roll process provides unique application potential—for example, in building architecture. Thin-film Si triple-junction cells in which amorphous and microcrystalline Si cells are stacked together have shown a record efficiency of 13.4% (*34*).

Quantum dot solar cells (efficiency 9.9%)

Quantum dot (QD) solar cells take advantage of the fact that semiconductor quantum dots can be synthesized using (low-temperature) solution processing, with their band gap tunable by composition and size. The best QD solar cells so far are made using PbS or PbSe QDs as the active layer. The QDs are deposited by spin coating or dip coating and then passivated and functionalized using organic molecules or halide salts. A p-n junction is made in the QD layer using a combination of surface ligands. QD cells are typically made on ITO- or FTO-coated glass, using a metal oxide (typically ZnO or TiO_2) as an electron-selective contact. Molybdenum oxide and Au or Ag are typically used as the back contact.

The record published efficiency for QD solar cells is 9.9% using PbS QDs with a band gap of 1.4 eV, with an architecture similar to previous work (*35*). The 9.9% cells have very large voltage loss (v = 0.56), the largest loss of all cells reviewed here, which is attributed to the fact that the QDs have a distribution of sizes that results in a distribution of band gap energies. In addition, a high density of radiative sub–band gap states and strong nonradiative surface recombination due to the large surface-to-volume ratio in the quantum dots (diameter ~5 nm) leads to recombination. Inefficient transport of carriers by hopping through the QD film limits the QD film thickness that can be practically used. Together, incomplete absorption and strong recombination contribute to a high current loss (j = 0.66). (Note that in the analysis we use the first excitonic peak in the absorption spectrum as the band gap of the quantum dots; taking a smaller electronic band gap correspondingly increases v and decreases j.)

Beyond the Shockley-Queisser limit

The S-Q detailed-balance model describes the efficiency limit for a single-junction solar cell under one-sun illumination. Efficiencies beyond the S-Q limit can potentially be achieved for a single-junction cell by using the process of multiple exciton generation (converting a single photon to multiple excitons, e.g., in quantum dots), by up- or down-conversion of incident light (to make the incident spectral range better match the semiconductor absorption spectrum), or by limiting the range of radiative emission angles (raising the cell voltage). So far, none of these "third-generation" PV concepts has led to an enhanced efficiency record for one of the PV materials described above.

Multijunction solar cells constitute a very broad field of research and are beyond the scope of this review (*36*). The highest reported efficiency under one-sun illumination is 38.8% for a GaInAs/GaInP/GaAs/AlGaInAs/AlGaInP five-junction tandem geometry (*37*). However, the manufacturing cost of such a complex cell architecture is very high.

Concentrating PV—that is, increasing the solar flux by focusing light on a solar cell—can (linearly) increase J_{sc} and (logarithmically) increase V_{oc}, leading to a higher efficiency. This concept is being applied in PV systems using macroscale lenses or parabolic mirrors in combination with ultrahigh-efficiency tandem cells. A record cell efficiency of 46.0% was measured using a GaInP/GaAs/GaInAsP/GaInAs tandem cell under 508× concentrated light. Concentrating PV requires a tracking system to follow the Sun and requires direct (rather than diffuse) sunlight.

Historical efficiency trends

There are large differences in the rate of efficiency improvement for the different materials discussed above. For example, after more than 60 years of research, single-crystalline Si is a mature technology, and the efficiency improvements that have been achieved in recent years have been relatively small and gradual. In contrast, the record efficiency for the new perovskite materials has climbed rapidly since the first cells were demonstrated, although cells with these record efficiencies are not yet stable in efficiency.

To illustrate recent trends in cell development, Fig. 5 compares present efficiencies with the average annual increase in absolute efficiency over recent years. Crystalline and multicrystalline Si have recently shown only gradual absolute efficiency improvements in the range of 0.04 to 0.09% per year; the increase in crystalline Si efficiencies results from progress in Si heterojunction cells. The high-efficiency thin-film materials perovskite (2.7% per year), CdTe (0.9% per year), and CIGS (0.2% per year) have made important steps forward over the past few years.

Although these recently demonstrated efficiency increases are no guarantee of improvements in the future, the realization of large yearly increases in materials with remaining room for growth in *v*, *j*, and *f* hints that research efforts have not yet become constrained by fundamental limits. Additional research will tell whether the record efficiency of CIGS, CdTe, or perovskite cells (now 4 to 5% below that of Si IBC cells) can exceed that of Si cells. The efficiency record for thin-film GaAs cells has not been broken since 2012; a more recent record is for thin-film III-V dual-junction cells (31.6%) (*29*). In the low-efficiency (10 to 12%) category, quantum dot solar cells (1.3% per year) and organic solar cells (0.6% per year) continue to make strong progress. Dye-sensitized cells and CZTS have not reported efficiency improvements since 2012 and 2013, respectively. We note that historically, when materials are developed to the level of commercialization, further efficiency increases are often observed beyond the records first achieved in a research laboratory. For example, the present efficiency records for Si IBC, GaAs, and CdTe cells are realized in manufacturing laboratories.

Solar module efficiencies

Two important factors create a gap between the record efficiency of laboratory solar cells and the record efficiency of laboratory modules or average efficiency of commercial modules, respectively. First, record-efficiency cells are often small-area devices made using specialized laboratory techniques that may be too expensive for large-scale production. For example, thin-film vacuum deposition of metal contacts may be used in the lab, while screen printing of contacts, leading to much lower metal conductivity, is used in industrial fabrication facilities. Second, modules are made of a number of larger-area cells connected in series and encapsulated. In the case of wafer-based technologies, incorporation of cells in a module inevitably leads to current loss (due to incomplete filling of the module area) and fill factor loss (due to additional resistance in cell interconnects and the use of larger cells). Optical effects upon encapsulation may decrease or increase efficiency, depending on the specifics of module design. Efficiencies of typical thin-film modules are lower than those of corresponding record cells because of the "dead area" associated with monolithic interconnection of strip-like cells, inhomogeneities or imperfections in the larger areas of the cells, and series resistance because of larger current transport distances.

Furthermore, in practice, solar modules never operate under conditions equal to the standard test conditions (STC). The solar spectrum and intensity change during the day and vary with the time of year. The dependence of efficiency on incident power is generally lowest for cells with high *FF*. Here the high-efficiency (mono)crystalline materials as well as thin-film CIGS and CdTe (all with $FF > 0.79$) have an advantage over perovskites and the lower-efficiency thin-film materials ($FF < 0.73$). Also, solar modules heat up under solar irradiation, sometimes reducing the efficiency by 1 to 2% (absolute) relative to their STC value defined at 25°C. The temperature coefficient of efficiency depends strongly on material and is lower for Si heterojunction cells, CdTe, and CIGS than for other materials (*38*, *39*). Another difference between practical, average module efficiency and STC efficiency is related to the fact that in practice modules receive light from a wide range of angles rather than perpendicularly incident light only. This leads to additional reflection losses. Finally, we note that nearly all cell/module combinations show reduction in efficiency over time. This is attributable to factors including degradation of the cells, oxidation of metallic cell interconnects, and photodegradation of polymer encapsulating layers; the magnitude of these effects depends on the cell/module combination (*40*). Understanding these degradation mechanisms in different climates is a complex but very important research challenge.

On the basis of their share in the market for PV systems, which had an estimated value of $96 billion in 2013 (*1*), it can be said that monocrystalline Si, multicrystalline Si, CdTe, and CIGS have evolved into mature high-efficiency technologies, with Si technology having >90% of the market share. Record efficiencies for large-area (>800 cm^2) modules are 22.4% for monocrystalline Si (*9*, *41*), 18.5% for multicrystalline Si (*9*), 18.6% for CdTe, and 17.5% for CIGS (*9*, *42*). These materials all belong to the >75% S-Q limit (for monocrystalline Si) or 50 to 75% S-Q limit (for multicrystalline Si, CIGS, CdTe) classes in Fig. 1B, directly demonstrating the importance of efficiency as a lever for large-scale application.

A recent development is the demonstration of single-junction GaAs solar modules with a record efficiency of 24.1% that are fabricated on an industrial scale and are now on their way to commercial exploitation (*43*). It will be interesting to see how the manufacturing costs for each of the >20% module technologies will decrease in the coming years. Thin-film solar cells deposited on thin foils are also expected to find new applications in areas where low weight-specific power (in terms of watts per gram) is desired, and in novel forms of building-integrated PV where flexible form factors or partial transparency for visible light are desired.

Thin-film amorphous and crystalline Si modules and flexible foils have also been developed to a commercial level but are applied on a much smaller scale because of their lower efficiency (12.2% for a module based on a tandem geometry) and higher manufacturing costs (*44*). Furthermore, small-area modules of dye-sensitized solar cells (efficiency 10.0%) (*45*, *46*) and organic solar cells (9.5%) (*30*) are commercially available but thus far represent a small market. Thin-film perovskite, CZTS, and quantum dot solar cells have been demonstrated in the lab, but modules have not yet been demonstrated on an industrial scale. For perovskites, long-term stability and manufacturability have not yet been demonstrated; for CZTS and quantum dot solar cells, the low efficiency limits its commercial development. Table 1 summarizes technological strengths and selected research technology opportunities for all reviewed materials.

Large-scale application of PV

The present worldwide primary energy supply through all sources (fossil, nuclear, and renewable) amounts to 18.0 TW; final consumption is 12.3 TW (*47*). In principle, this energy need can be fully met using PV, in combination with proper energy transport and storage systems and secondary conversion into heat and fuels. Assuming a modest module efficiency of 20%, a system capacity factor of 15%, an average ground cover ratio of 50%, and 50% losses related to storage and secondary conversion, 1.6% of Earth's land area would be required to produce an amount of energy equal to the current primary supply. Although in absolute terms this is a very large number, it is not unrealistic. To put this in perspective, this area is less than 5% of the area used for agriculture worldwide. Also, note that substantial land areas are already used today for production of fossil fuels and various types of biofuel. Finally, by drastically increasing the efficiency of solar modules,

Table 1. Technology strengths and key research opportunities for photovoltaic materials. Materials are grouped by degree of technological development. Record cell and module efficiencies are indicated, based on certified measurements. GaInP and InP are not included as no significant development toward commercial technology exists; n.a., not available.

Material	Cell efficiency (%)	Module efficiency (%)	Technology strengths and options	Selected research/technology opportunities
Mature technologies deployed at large scale				
Monocrystalline Si	25.6	22.4	Earth-abundant material; >25-year track record	Further reduce recombination losses, in combination with new metallization schemes; improve light management in thinner wafers; improve IBC and SHJ cell designs
Multicrystalline Si	21.3	18.5	Earth-abundant material; >25-year track record	Improve wafer quality (minimize or passivate defects) to reduce recombination losses
CIGS	21.7	17.5	Flexible substrates	Improve light management; increase efficiency for large band gaps (tandem cells); reduce recombination losses, solution processing
CdTe	21.5	18.6	Flexible substrates; short energy payback time	Reduce recombination losses; develop thinner cell designs using light management
Emerging technologies deployed at smaller scale				
Dye-sensitized TiO_2	11.9	10.0	Tunable colors	Improve redox couple; reduce recombination losses; increase band gap; increase stability
Thin-film Si	11.4	12.2*	Flexible modules	Reduce recombination losses; improve light management
Organic	11.5	9.5	Flexible modules, semitransparent modules	Improve light management; increase band gap; increase stability; reduce recombination losses
Technology at the manufacturing level				
GaAs	28.8	24.1	Very high efficiency; flexible modules	Improve light management; develop IBC geometry; further develop thin-film multijunction cells by layer transfer
Technologies under development				
Perovskite	21.0	n.a.	Solution processing; flexible modules	Reduce recombination losses; improve cell stability; avoid use of Pb; increase efficiency for high–band gap materials (tandem cells); develop Si/perovskite tandems
CZTS	12.6	n.a.	Flexible modules	Reduce recombination losses; improve light management
Quantum dots	9.9	n.a.	Solution processing; flexible modules	Reduce recombination losses; improve light management; avoid use of Pb

*Microcrystalline Si/a-Si tandem geometry.

by integrating PV into buildings and other objects, and by combining PV technology with other renewable sources such as solar thermal energy and wind energy, a much smaller land area would be needed.

For PV to break through at such a large scale, a further reduction in costs of PV technology is required. As stated above, increasing cell efficiency is a key driver for reducing costs, as the costs of the solar cells themselves constitute only part (<50%) of the costs of a full PV system. Furthermore, the overall cost of PV systems will decrease by economy of scale as production capacity and installation volumes are further increased. Scalability of technology and availability of raw materials are essential parameters, as are the energy costs of fabricating PV systems at a large scale. Long lifetime and stable operation are additional crucial parameters, as is design-for-recycling, which allows valuable or toxic materials to be recovered in a practical way.

Future research directions: Light management and carrier management

We have categorized the architectures of 16 PV materials in terms of their current and voltage losses relative to the S-Q limiting values. To further increase the photocurrent in a particular cell design typically requires better management of light in order to reduce reflection, reduce parasitic absorption, and enhance light trapping in the active area of the cell. Nanophotonic concepts, in which nanostructures with typical length scales equal to or smaller than the wavelength of light are incorporated in the solar cell, can serve to reach these goals (*5*, *48*–*50*). Such structures can preferentially scatter and confine light so that it is better absorbed in the cell. Nanophotonic concepts leading to enhanced light trapping can also

reduce the required material thickness, thereby reducing bulk recombination (which enhances the voltage) and reducing costs. Nanophotonic control can also enhance the voltage by reducing entropic losses via control of the angular distribution of light emission from the cell. Large-area engineered nanopatterns integrated in solar cells can be made using soft-imprint technology that can be scaled up to the square-kilometer areas required for large-area production. We predict that further advances in nanophotovoltaics will lead to enhanced photocurrents, and thus enhanced efficiency, in several different PV materials and architectures. Nanophotonic concepts can also be used to engineer the color of solar panels, providing many new opportunities for building-integrated PV.

Improving the cell voltage and fill factor requires detailed understanding of and control over carrier recombination mechanisms in the cell. Making advances in the quality of electrical materials constitutes a major engineering research effort that involves identification of bulk, interface, and surface defects, as well as measurement of their density, energy levels, formation energy, annealing characteristics, passivation behavior, dopant diffusion, contact formation, and many other properties. The realization of high-quality PV materials that enable low-cost manufacturing of solar cells with efficiencies approaching the S-Q limit will require a coordinated international materials science and engineering approach.

Conclusions and outlook

The record efficiency of single-junction solar cells has continually increased over the years, but so far no PV material has closely approached the theoretical S-Q efficiency limit. Monocrystalline Si and GaAs have reached efficiencies of 26 to 29%; several polycrystalline materials (Si, CIGS, CdTe, perovskite) are in the 20 to 22% range; and all other common thin-film materials have efficiencies in the 10 to 13% range. There is much room for improvement in all of the materials discussed, and there is no doubt that efficiency records will continue to be broken in the future (*28*). The lower-efficiency (flexible) materials can find applications in building-integrated PV systems, flexible electronics, flexible power generation systems, and many other (sometimes niche) markets. High-efficiency (>20%) materials can find applications in large-area PV power generation for the utility grid, as well as in small and medium-sized systems for the built environment. They will enable very large-scale penetration into our energy system, starting now and growing as the cost per kilowatt-hour is reduced further by a factor of 2 to 3. This can be achieved by advanced (nanophotonic) cell designs in combination with an extensive materials science and engineering effort to further enhance PV material quality.

REFERENCES AND NOTES

1. *Technology Roadmap: Solar Photovoltaic Energy (2014 Edition)* (International Energy Agency, Paris, 2014).
2. W. Shockley, H. J. Queisser, Detailed balance limit of efficiency of p-n junction solar cells. *J. Appl. Phys.* **32**, 510–519 (1961). doi: 10.1063/1.1736034
3. T. Tiedje, Band tail recombination limit to the output voltage of amorphous silicon solar cells. *Appl. Phys. Lett.* **40**, 627–629 (1982). doi: 10.1063/1.93168
4. U. Rau, J. H. Werner, Radiative efficiency limits of solar cells with lateral band-gap fluctuations. *Appl. Phys. Lett.* **84**, 3735–3737 (2004). doi: 10.1063/1.1737071
5. U. Rau, U. W. Paetzold, T. Kirchartz, Thermodynamics of light management in photovoltaic devices. *Phys. Rev. B* **90**, 035211 (2014). doi: 10.1103/PhysRevB.90.035211
6. M. Topic, R. M. Geisthardt, J. R. Sites, Performance limits and status of single-junction solar cells with emphasis on CIGS. *IEEE J. Photovolt.* **5**, 360–365 (2015). doi: 10.1109/JPHOTOV.2014.2359135
7. S. W. Glunz *et al*., The irresistible charm of a simple current flow pattern — 25% with a solar cell featuring a full-area back contact. In *Proceedings of the 31st European Photovoltaic Solar Energy Conference and Exhibition*, 259–263 (2015). doi: 10.4229/EUPVSEC20152015-2BP.1.1
8. J. Zhao, A. Wang, M. A. Green, F. Ferrazza, 19.8% efficient "honeycomb" textured multicrystalline and 24.4% monocrystalline silicon solar cells. *Appl. Phys. Lett.* **73**, 1991–1993 (1998). doi: 10.1063/1.122345
9. M. A. Green, K. Emery, Y. Hishikawa, W. Warta, E. D. Dunlop, Solar cell efficiency tables (version 45). *Prog. Photovolt. Res. Appl.* **23**, 1–9 (2015). doi: 10.1002/pip.2573
10. P. J. Cousins *et al*., Gen III: Improved performance at lower cost. In *Proceedings of the IEEE Photovoltaic Specialists Conference (PVSC)*, 275–278 (2010). doi: 10.1109/PVSC.2010.5615850
11. M. A. Green, K. Emery, Y. Hishikawa, W. Warta, E. D. Dunlop, Solar cell efficiency tables (version 47). *Prog. Photovolt. Res. Appl.* **24**, 3–11 (2016). doi: 10.1002/pip.2728
12. Panasonic press release: Panasonic HIT® solar cell achieves world's highest energy conversion efficiency of 25.6% at research level (10 April 2014); http://news.panasonic.com/press/news/official.data/data.dir/2014/04/en140410-4/en140410-4.html.
13. P. J. Verlinden *et al*., "Strategy, development and mass production of high-efficiency crystalline Si PV modules." Presented at 6th World Conference on PV Energy Conversion, Kyoto, November 2014.
14. A. Richter, M. Hermle, S. W. Glunz, Reassessment of the limiting efficiency for crystalline silicon solar cells. *IEEE J. Photovolt.* **3**, 1184–1191 (2013). doi: 10.1109/JPHOTOV.2013.2270351
15. D. D. Smith *et al*., Generation III high efficiency lower cost technology: Transition to full scale manufacturing. In *Proceedings of the 38th IEEE Photovoltaic Specialists Conference (PVSC)*, 1594–1597 (2012). doi: 10.1109/PVSC.2012.6317899
16. B. M. Kayes *et al*., 27.6% conversion efficiency, a new record for single-junction solar cells under 1 sun illumination. In *Proceedings of the 37th IEEE Photovoltaic Specialists Conference (PVSC)*, 4–8 (2011). doi: 10.1109/PVSC.2011.6185831
17. E. D. Kosten, J. H. Atwater, J. Parsons, A. Polman, H. A. Atwater, Highly efficient GaAs solar cells by limiting light emission angle. *Light Sci. Appl.* **2**, e45 (2013). doi: 10.1038/lsa.2013.1
18. C. J. Keavney, V. E. Haven, S. M. Vernon, Emitter structures in MOCVD InP solar cells. In *Conference Record of the 21st IEEE Photovoltaic Specialists Conference (PVSC)* **1**, 141–144 (1990). doi: 10.1109/PVSC.1990.111606
19. J. F. Geisz, M. A. Steiner, I. Garcia, S. R. Kurtz, D. J. Friedman, Enhanced external radiative efficiency for 20.8% efficient single-junction GaInP solar cells. *Appl. Phys. Lett.* **103**, 041118 (2013). doi: 10.1063/1.4816837
20. P. Jackson *et al*., Properties of Cu(In,Ga)Se_2 solar cells with new record efficiencies up to 21.7%. *Phys. Status Solidi RRL* **9**, 28–31 (2015). doi: 10.1002/pssr.201409520
21. First Solar press release: "First Solar achieves efficiency, durability milestones" (5 February 2015); http://investor.firstsolar.com/releasedetail.cfm?ReleaseID=895118.
22. First Solar press release: "First Solar builds the highest efficiency thin film PV cell on record" (5 August 2014); http://investor.firstsolar.com/releasedetail.cfm?ReleaseID=864426.
23. G. Xing *et al*., Low-temperature solution-processed wavelength-tunable perovskites for lasing. *Nat. Mater.* **13**, 476–480 (2014). doi: 10.1038/nmat3911; pmid: 24633346
24. N. J. Jeon *et al*., Compositional engineering of perovskite materials for high-performance solar cells. *Nature* **517**, 476–480 (2015). doi: 10.1038/nature14133; pmid: 25561177
25. T. K. Todorov, K. B. Reuter, D. B. Mitzi, High-efficiency solar cell with Earth-abundant liquid-processed absorber. *Adv. Mater.* **22**, E156–E159 (2010). doi: 10.1002/adma.200904155; pmid: 20641095
26. W. Wang *et al*., Device characteristics of CZTSSe thin-film solar cells with 12.6% efficiency. *Adv. Energy Mater.* **4**, 1301465 (2014). doi: 10.1002/aenm.201301465
27. R. Komiya *et al*., Improvement of the conversion efficiency of a monolithic type dye-sensitized solar cell module. *Technical Digest, 21st International Photovoltaic Science and Engineering Conference, Fukuoka, Japan* **2**, C-5O-08 (2011).
28. An overview of all records with updated values for current and voltage relative to the S-Q limits (table S1) is kept up to date on http://lmpv.amolf.nl/SQ.
29. National Renewable Energy Laboratory, Best Research-Cell Efficiencies; www.nrel.gov/ncpv/images/efficiency_chart.jpg (2016).
30. M. Hosoya *et al*., "Module development for polymer solar cells (abstract O-Pv-6-2)." Presented at the Grand Renewable Energy Conference, Tokyo, July 2014.
31. T. Kirchartz, K. Taretto, U. Rau, Efficiency limits of organic bulk heterojunction solar cells. *J. Phys. Chem. C* **113**, 17958–17966 (2009). doi: 10.1021/jp906292h
32. H. Sai, T. Matsui, K. Matsubara, M. Kondo, I. Yoshida, 11.0%-efficient thin-film microcrystalline silicon solar cells with honeycomb textured substrates. *IEEE J. Photovolt.* **4**, 1349–1353 (2014). doi: 10.1109/JPHOTOV.2014.2355037
33. T. Matsui *et al*., Development of highly stable and efficient amorphous silicon based solar cells. In *Proceedings of the 28th European Photovoltaic Solar Energy Conference and Exhibition*, 2213–2217 (2013). doi: 10.4229/28thEUPVSEC2013-3DO.7.2
34. S.-W. Ahn, S.-E. Lee, H. M. Lee, "Toward commercialization of triple-junction thin-film silicon solar panel with >12% efficiency." Presented at the 37th PVSEC Conference, Frankfurt, September 2012.
35. C.-H. M. Chuang, P. R. Brown, V. Bulović, M. G. Bawendi, Improved performance and stability in quantum dot solar cells through band alignment engineering. *Nat. Mater.* **13**, 796–801 (2014). doi: 10.1038/nmat3984; pmid: 24859641
36. K. Tanabe, A review of ultrahigh efficiency III-V semiconductor compound solar cells: Multijunction tandem, lower dimensional, photonic up/down conversion and plasmonic nanometallic structures. *Energies* **2**, 504–530 (2009). doi: 10.3390/en20300504
37. P. T. Chiu *et al*., 35.8% space and 38.8% terrestrial 5j direct bonded cells. In *Proceedings of the 40th IEEE Photovoltaic Specialist Conference (PVSC)*, 11–13 (2014). doi: 10.1109/PVSC.2014.6924957
38. A. Virtuani, D. Pavanello, G. Friesen, Overview of temperature coefficients of different thin film photovoltaic materials. In *Proceedings of the 25th European Photovoltaic Solar Energy Conference and Exhibition*, 4248–4252 (2010). doi: 10.4229/25thEUPVSEC2010-4AV.3.83
39. T. Mishima, M. Taguchi, H. Sakata, E. Maruyama, Development status of high-efficiency HIT solar cells. *Sol. Energy Mater. Sol. Cells* **95**, 18–21 (2011). doi: 10.1016/j.solmat.2010.04.030
40. R. Jones-Albertus, D. Feldman, R. Fu, K. Horowitz, M. Woodhouse, "Technology advances needed for photovoltaics to achieve widespread grid price parity" (2016); http://energy.gov/eere/sunshot/downloads/technology-advances-needed-photovoltaics-achieve-widespread-grid-price-parity.
41. R. Swanson, "The role of modeling in SunPower's commercialisation efforts." Presented at the Workshop on Challenges in PV Science, Technology, and Manufacturing, West Lafayette, IN, August 2012.
42. H. Sugimoto, High efficiency and large volume production of CIS-based modules. In *Proceedings of the 40th IEEE Photovoltaic Specialist Conference (PVSC)*, 2767–2770 (2014). doi: 10.1109/PVSC.2014.6925503
43. H. Sai *et al*., Microcrystalline silicon solar cells with 10.5% efficiency realized by improved photon absorption via periodic textures and highly transparent conductive oxide. *Appl. Phys. Express* **6**, 104101 (2013). doi: 10.7567/APEX.6.104101
44. Tel Solar press release: "New record-breaking PV module efficiency has been achieved" (9 July 2014); www.solar.tel.com.
45. H. Ozawa, Y. Okuyama, H. Arakawa, Dependence of the efficiency improvement of black-dye-based dye-sensitized solar cells on alkyl chain length of quaternary ammonium cations in electrolyte solutions. *ChemPhysChem* **15**, 1201–1206 (2014). doi: 10.1002/cphc.201301025; pmid: 24482147

46. N. Tanabe, Dye sensitized solar cell for energy harvesting applications. *Fujikura Tech. Rev.* **42**, 109–113 (2013); www.fujikura.co.jp/eng/rd/gihou/2048261_11754.html.
47. International Energy Agency, Key World Energy Statistics (2015); www.iea.org/publications/freepublications/publication/key-world-energy-statistics-2015.html.
48. H. A. Atwater, A. Polman, Plasmonics for improved photovoltaic devices. *Nat. Mater.* **9**, 205–213 (2010). doi: 10.1038/nmat2629; pmid: 20168344
49. M. L. Brongersma, Y. Cui, S. Fan, Light management for photovoltaics using high-index nanostructures. *Nat. Mater.* **13**, 451–460 (2014). doi: 10.1038/nmat3921; pmid: 24751773
50. A. Polman, H. A. Atwater, Photonic design principles for ultrahigh-efficiency photovoltaics. *Nat. Mater.* **11**, 174–177 (2012). doi: 10.1038/nmat3263; pmid: 22349847

ACKNOWLEDGMENTS

This work is part of the research program of the Foundation for Fundamental Research on Matter (FOM), which is part of the Netherlands Organisation for Scientific Research (NWO). It is also supported by NanoNextNL, a nanotechnology program of the Dutch ministry of economic affairs, the European Research Council, and the Global Climate and Energy Project. The authors declare no competing financial interests. The data are archived in the laboratory of A.P. The data in table S1 will be continuously updated and made available on http://lmpv.amolf.nl/SQ.

SUPPLEMENTARY MATERIALS

www.sciencemag.org/content/352/6283/aad4424/suppl/DC1
Table S1
References (*51*–*56*)

10.1126/science.aad4424